Initial Nucleation of Au on the $(\sqrt{2} \times \sqrt{2})$R45° Reconstructed Fe_3O_4(001) Surface

K. Jordan, [1] S. Murphy and I. V. Shvets.

Centre for Research on Adaptive Nanostructures and Nanodevices (CRANN) & School of Physics, Trinity College, Dublin 2, Ireland.

Abstract

The initial nucleation of Au onto the $(\sqrt{2} \times \sqrt{2})$R45° reconstructed Fe_3O_4(001) surface has been studied using scanning tunneling microscopy. Au clusters are formed, with a typical lateral dimension of $\sim$ 9 Å. The measured corrugation height of the clusters, $\sim$ 1 Å, suggests that they are a single atomic layer in height. The clusters nucleate on a specific surface site, which lies at the centre of a $(\sqrt{2} \times \sqrt{2})$R45° reconstructed unit cell. The size and spatial distribution of the Au clusters formed is shown to strongly correlate to the symmetry and periodicity of the reconstructed magnetite surface. It is also shown that even when the clusters are in close proximity they still only occupy this single nucleation site, and thus maintain the periodicity of the substrate. We relate the order and stability of this system to the fact that magnetite (001) is polar, and suggest that such surfaces offer ideal templates for self-assembly due to the stability of their polarity induced reconstructions.

Key words: scanning tunnelling microscopy, oxide surface, polar surface, self-assembly, clusters
PACS: 68.37.Ef, 68.35.Dv, 68.47.Jn, 81.16.Dn

1 Introduction

The nucleation of nanoscale metal clusters onto oxide surfaces is an area of great interest. Aside from the novel electronic and magnetic properties that can arise due to the low dimensionality of nanostructures [1], this intense interest is driven mainly by the fact that metals which are inert in bulk form, for example Au, can exhibit high catalytic activity when in the form of nanoscale clusters supported on metal oxide substrates [2,3]. This catalytic behaviour is

[1] Corresponding Author. Fax: + 353 1 671 1759; e-mail: jordank@tcd.ie

thought to be highly dependent on issues such as cluster size, binding site, and charge transfer between the clusters and substrate [4]. It has been shown that oxygen vacancies on metal oxide surfaces can act as active nucleation sites for metal clusters, greatly altering the adsorption of metals compared to defect free surfaces [5–11]. Furthermore, it has explicitly been shown that these vacancies play a vital role in the catalytic activity of such systems [12,13]. Indeed, it was recently found that Au octomers bound to oxygen vacancy defects on MgO(001) catalyse the low temperature oxidation of CO to CO_2, whereas those clusters bound to defect free MgO(001) are chemically inert [14].

In terms of the growth mode of these nanoscale clusters, it is known that the process of nucleation is dependent on an interplay of adsorbate-adsorbate and adsorbate-substrate interactions. It has been shown that one can exploit the alternating potential landscape of surface reconstructions to achieve the growth of metal clusters with well defined size and spatial distribution [15]. In particular, cluster growth on an oxide surface has been demonstrated for numerous metals, including Au, using Al_2O_3 thin films grown on $Ni_3Al(111)$ [16]. It is also recognised that, as mentioned in the previous paragraph, surface oxygen vacancy defects can have an extremely important role to play in the formation of nanoscale metal clusters on oxide surfaces [8,9]. These previous studies have been on surfaces which exhibit random vacancy formation. However, some surfaces can exhibit long range ordered oxygen vacancy networks, formed over the entirety of the surface. The possibility of using such surfaces as a template for the production of nanocluster arrays with long range order has not yet been investigated. Polar crystal faces are the ideal candidates for such work. According to Tasker [17,18], such surfaces must reconstruct in order to eliminate a diverging dipole moment that results from the fact that the crystal is formed from alternating layers with opposite charge. One possibility is that the reconstruction can take the form of actual ion vacancies, such that the charge of the two identical surface layers is halved, which eliminates polarity. This type of vacancy surface reconstruction clearly differs markedly to, for example, the well known rearrangement of dangling bonds that can occur at semiconductor surfaces or the changes in interatomic spacing that can occur at metal surfaces. Whereas the former occurs due to a diverging energy caused by the polarity of certain crystals [17,18], the latter are driven only by a reduction of surface energy.

Magnetite (001) constitutes one such polar crystal. The alternately stacked octahedral and tetrahedral layers have equal and opposite charge. To eliminate polarity the overall charge of the identical surface layers must be halved. From successive STM studies [19–22] and, more recently, DFT calculations [23,24] it is now accepted that the surface terminates at the octahedral plane. A schematic of the unreconstructed octahedral surface is shown in Fig.1(a). For the octahedral plane the polarity induced reconstruction can consist of a reduction in the number of O^{2-} species. As first pointed out by Voogt [25],

the formation of one O^{2-} vacancy per $(\sqrt{2} \times \sqrt{2})$R45° unit cell greatly moves the surface toward polarity cancellation, and also agrees with the observed $(\sqrt{2} \times \sqrt{2})$R45° low energy electron diffraction (LEED) mesh. Later STM work by Stanka [19] again revealed a $(\sqrt{2} \times \sqrt{2})$R45° symmetry and showed that the Fe_{oct} rows had a zig-zag structure along the [110] direction, possibly due to the repulsive effect that the proposed oxygen vacancies would have on the [110] oriented rows. A schematic of this structure is shown in Fig.1(b). In terms of the electrostatic model of polar surfaces [17,18], this $(\sqrt{2} \times \sqrt{2})$R45° array of oxygen vacancies best explains the observed results. However, more recently, alternative models have been put forward to explain the $(\sqrt{2} \times \sqrt{2})$R45° symmetry. It has been proposed that the $(\sqrt{2} \times \sqrt{2})$R45° reconstruction is not due to an ordered array of oxygen vacancies, but could be due to deformations of the oxygen fcc lattice at the surface [26]. Such distortions could also give rise to a lateral shifting of the octahedral Fe ions, yielding a $(\sqrt{2} \times \sqrt{2})$R45° surface symmetry [24]. It should be noted that such models, which do not involve any change in the overall charge of the surface layers, cannot possibly satisfy the electrostatic model of polar surfaces. Our extensive experience with studies of the Fe_3O_4(001) surface suggest that the surface reconstruction formed can depend on the preparation conditions, primarily anneal temperature and oxygen partial pressure. It is possible that there are different reconstructions with comparable energy which are metastable. Therefore several models of the surface termination may be equally valid, and depend on the finer details of the preparation procedure.

In this work we study the initial nucleation of Au onto the $(\sqrt{2} \times \sqrt{2})$R45° reconstructed magnetite (001) surface. The gold forms uniformly sized clusters, which preferentially nucleate on a single surface site. The location of this site is in-keeping with the periodicity of the surface reconstruction, illustrating that the adsorption energy is modulated across the magnetite (001) surface by the reconstruction. We suggest that the $(\sqrt{2} \times \sqrt{2})$R45° reconstruction, incorporating oxygen vacancies, acts as a template for the self-organised nucleation of Au clusters.

2 Experimental

A synthetic Fe_3O_4 single crystal was used for these experiments. Four wire resistivity *vs.* temperature measurements on the single crystals revealed a Verwey transition temperature (T_v) $\sim$ 120 K. The crystal was cut along the <010> direction to an accuracy of 1° and polished using diamond paste of decreasing grain size, down to a grain size of 0.25 μm. Experiments were performed in a multichamber UHV system, with a base pressure of 1×10^{-10} Torr. The in-situ sample preparation consisted of cycles of Ar^+ ion etching and post-annealing in oxygen partial pressure of 2×10^{-6} Torr for 30 minutes.

This sample preparation routinely results in a clean surface, as determined by Auger electron spectroscopy (AES), displaying a sharp $(\sqrt{2}\times\sqrt{2})$R45° LEED pattern. Ultrapure Au was evaporated, from a molybdenum crucible, using an electron-beam evaporator. The chamber pressure did not exceed 8×10^{-10} Torr during evaporation. Deposition rates were ascertained using a quartz crystal balance. The STM measurements presented here were carried out at room temperature, in constant current mode, using a home built instrument in conjunction with a commercial Omicron Scala STM controller. Except where stated otherwise, electrochemically etched W tips, prepared as described in reference [27], were used for STM.

3 Results and Discussion

3.1 The Clean $(\sqrt{2}\times\sqrt{2})R45°$ Reconstructed Magnetite Surface

The clean magnetite (001) surface, prepared as described above, exhibits a $(\sqrt{2}\times\sqrt{2})$R45° reconstruction. As noted in previous studies [19–21,28], the surface is in agreement with termination at the octahedral plane. The fine structure of the surface is revealed by high resolution images. As the O_{2p} levels lie far below the Fermi level, the resolved atoms are the octahedral irons [29]. Fig. 2(a) presents an image obtained with a MnNi tip. Three types of feature are resolved within a single 8.4×8.4 Å^2 unit cell; A bright point labelled α, a less bright point labelled β, and finally, a local depression labelled γ. The local depressions constitute the four corners of the unit cell outlined in Fig. 2(a). As explained in reference [28], it is likely that the differing bright points correspond to Fe-Fe dimers of different charge. As previously proposed by Stanka *et al.*[19] the local depression can be explained in terms of a single oxygen vacancy per surface $(\sqrt{2}\times\sqrt{2})$R45° unit cell and the repulsive effect that this vacancy site would have on the surrounding Fe cations can explain the wave-like structure of the Fe rows along [110], which is evident from the line profile along the $[1\bar{1}0]$ direction [Fig.2(b)]. We further note that, as stated in reference [28], when the surface is imaged with W tips, one does not observe the bright and less bright points. Instead they are imaged as one large bright point [Fig. 2(c)]. This large bright point can be thought of as two Fe-Fe dimers shifted toward each other along the $[1\bar{1}0]$ direction. This results in an apparent 12 Å periodicity, as seen in Fig. 2(d). The $(\sqrt{2}\times\sqrt{2})$R45° array of depressions is imaged with either tip material. The exact same unit cell is outlined in both STM images, with a dashed white square. It is also worth noting that the images of the clean surface presented here show that the atomic corrugation of the magnetite (001) surface is strongly dependent on the junction polarity, with a much larger corrugation height evident for a sample bias of -1V compared to +1V. This junction polarity dependant cor-

rugation has been observed to be independent of the tip. This is indicative that a complex non-metal like density of states is maintained at the magnetite (001) surface, which has been confirmed with STS experiments [30]

The STM results support the model of Stanka *et al.* [19], which is based on an $(\sqrt{2}\times\sqrt{2})$R45° array of oxygen vacancies, with however, the incorporation of dimerisation and a degree of surface charge ordering. As seen from Fig. 1(b), the four corners of a unit cell are centred on oxygen vacancies. The centre of the cell is then occupied by two Fe-Fe dimers of differing charge. This cell agrees well with the unit cell outlined in the STM images, where the four corners of the cell are centred on local depressions, and two Fe-Fe dimers occupy the centre of the cell.

3.2 Initial Nucleation of Au on $(\sqrt{2}\times\sqrt{2})R45°$ Reconstructed Magnetite Surface

Using a 0.008 Ås^{-1} deposition rate ∼0.03 ML of Au was deposited onto the $(\sqrt{2}\times\sqrt{2})$R45° reconstructed magnetite (001) surface. An STM image of the surface following such a deposition is shown in Fig. 3(a). Au clusters form on the surface. From the line profiles presented in Fig. 3, it can be seen that the clusters have an apparent radius of ∼9 Å. They have an apparent height of ∼1 Å, suggesting that they consist of a single monolayer of Au. As can be seen from the images, the cluster size is quite uniform, with only 10-15% of clusters being of larger dimensions on well ordered terraces. We note that there is some evidence of a slight elongation of the clusters, however the direction of elongation is not very reproducible and appears to be dependent on the scan direction. We also note that the reported dimensions are apparent dimensions, and that the size of such clusters in STM depends not only on the actual size, but on the electronic structure of the cluster, and cluster-substrate interactions. Therefore the clusters may be composed of far less atoms than the size seen here suggests. The exact registry of the Au clusters, with respect to the $(\sqrt{2}\times\sqrt{2})$R45° reconstructed magnetite surface, can be extracted from the presented line profiles. Close examination of the STM image shows that the Au clusters are always positioned such that they are at the centre of four local depressions, which form the corners of the previously outlined $(\sqrt{2}\times\sqrt{2})$R45° unit cell. The presented line profiles further validate this point. The line profile (i) is taken along an area with no cluster present. The line profile (ii) is an equivalent line profile in the presence of a Au cluster. It can be seen that the maximum of the cluster corresponds to a maximum in the line profile (i). The same is true for line profiles in the perpendicular direction. These maxima correspond to the centre of the outlined $(\sqrt{2}\times\sqrt{2})$R45° unit cell of the substrate.

A higher resolution STM image of a similar surface is presented in Fig 4(a). In this image the underlying magnetite (001) substrate is better resolved. The bright points imaged, which we recall constitute two Fe dimers that converge together along the $[1\bar{1}0]$ direction, are elongated along this direction, as seen earlier for the clean surface in Fig. 2(c). It is more clearly seen from this higher resolution image that the Au clusters nucleate at the centre of the $(\sqrt{2}\times\sqrt{2})$R45° unit cell, with the four corners of the cell centred on local depressions, as outlined by the dashed black square in Fig. 4(a). This nucleation site is presented schematically, with respect to the $(\sqrt{2}\times\sqrt{2})$R45° reconstructed surface with an array of oxygen vacancies, in Fig. 4(c). The fact that there is a single unique nucleation site on the surface, which is the centre of a $(\sqrt{2}\times\sqrt{2})$R45° reconstructed unit cell, manifests itself in that the imaged Au clusters are always separated by multiples of 12 Å along the [110] and $[1\bar{1}0]$ directions. This point is further evident from Fig. 4(d), where a mesh of $(\sqrt{2}\times\sqrt{2})$R45° unit cells is drawn over the surface and it can be seen that the Au clusters always nucleate at the centre of these cells.

Au clusters in close proximity to each other have also been imaged. Fig. 5, presents an STM image of an area of the surface where four Au clusters have nucleated on directly adjacent unit cells. The dashed black square outlines the unit cell previously identified. An alternative 8.4×8.4 Å^2 surface unit cell can also be identified, with the four corners centered on each of the Au clusters. This is outlined by the grey dashed cell in Fig. 5(a). A schematic of the cluster arrangement is shown in Fig. 5(b). The important point to note is that, despite their proximity, the clusters are still discretely resolved, and they still occupy the identified site.

3.3 Discussion

The images of Au nucleation presented show that the $(\sqrt{2}\times\sqrt{2})$R45° reconstructed magnetite (001) surface acts as a template for the nucleation of nanoscale Au clusters. The template effect results from the fact that a single surface site is highly preferable as a nucleation center compared to other surface sites. This site can be thought of as the centre of a $(\sqrt{2}\times\sqrt{2})$R45° surface unit cell, which has an oxygen vacancy at each of the four corners. As a result of there being a single nucleation site the clusters have a spacing in-keeping with the periodicity of the reconstruction. The fact that the clusters nucleate within the centre of a unit cell site also leads to a fairly uniform cluster size. The stability of the clusters occupying this site is also an interesting aspect of this system. The most obvious reason for the stability of uniformly sized clusters, occupying a single surface site, is that it is due to a periodic variation in the surface potential that arises from the ordered array of oxygen vacancies. This vacancy array hinders diffusion of the Au clusters across the surface,

making a merging of the clusters energetically unfavourable.

From the images it is clear that, for this system, the Au clusters do not bind directly to the oxygen vacancy site itself. Instead they nucleate on the site which is surrounded by the vacancies. We note that it has previously been shown that oxygen vacancies on TiO_2(110) and MgO(001) can be favourable nucleation sites for Au and Pd respectively [8,9]. Recent work has also suggested that reduced Ti sites on TiO_x may play a role as an active site for nucleation and growth of Au clusters on the surface [31]. The somewhat contrasting results obtained for the Fe_3O_4(001) surface may be due to the fact that these previous studies were for the case of atoms and clusters binding to unordered surface O vacancies. Unordered vacancies will not result in a long range alterations to the topographic and electronic structure of a surface, or the creation of periodic adsorption potential of the type that can be caused by a reconstruction. Indeed, the site identified here as the favoured one would not even exist in the case of an isolated O vacancy. Therefore, the situation for a surface with random isolated oxygen vacancies compared to a periodic array is entirely different.

There are, in our view, two possibilities for the identified site being favoured. A combination of these two mechanisms may also be occurring. The first is that there is a periodic surface stress that makes this site a potential well for the Au cluster. The second is that there is a charge redistribution due to the vacancy array. The O vacancy sites take on a virtual positive charge of 2+, thus becoming highly electron deficient. The nucleation site identified will be relatively electron rich, compared to the vacancy site. Intuitively, this should favour nucleation of the relatively electronegative Au (2.54/Pauling unit [32]) on this site. This argument applies only to the situation presented here; that is, a long range ordered vacancy array. Again the situation for unordered vacancies is entirely different, as the non-periodic nature of the surface will lead to a far more complicated situation, with a much greater variety and number of different surface sites that are potential binding sites.

It is clear that the periodically varying adsorption potential of the surface plays a vital role in the size of the clusters and the existence of a favourable nucleation site, which maps out the periodicity of the substrate reconstruction. The fact that Au clusters do not coalesce, even when in close proximity [Fig5], can also be attributed to this periodically varying surface potential. If it is the case that attractive interactions exist between the Au clusters, the STM images show that the diffusion barrier is greater than any such interactions that may exist. A repulsive cluster-cluster interaction has previously been used to explain the ordered nucleation of Au atoms onto the FeO(111) surface, with this interaction said to dictate the minimum achievable separation [33]. However, for the system studied here, the separation of the clusters is in-keeping with the periodicity of the substrate reconstruction, suggesting that

such repulsive interactions do not dominate over the periodic potential of the substrate surface in limiting the separation of the clusters.

The stability of the $(\sqrt{2} \times \sqrt{2})$R45° surface reconstruction, despite the nucleation of Au, is borne out by the fact that the $(\sqrt{2} \times \sqrt{2})$R45° LEED mesh remains even for Au coverages close to 1ML. This stability is best explained by the fact that magnetite (001) is a polar surface. Effects caused by nucleation on a surface, such as induced surface stress or charge transfer, are known to alter surface reconstructions which have a suitably low stabilisation energy, for example surfaces whose reconstructions are driven solely by surface energy minimisation concerns. However, polar surfaces, such as magnetite (001) reconstruct in order to eliminate a diverging energy [17,18]. Therefore, the driving force behind such reconstructions is of far greater energy than those formed due to purely surface energy concerns. Furthermore, it is inherent in the electrostatic model of polar surfaces that following the nucleation of charge nuetral species the reconstruction remains stable. This is because the overall charge of the terminal surface plane is unchanged following the adsorption of charge neutral species. Therefore the driving force behind the reconstruction is also unchanged, and so the reconstruction will remain stable following nucleation of uncharged species, in theory allowing self assembly to continue even for high cluster coverages. Such reconstructed surfaces of polar crystals offer unparalleled stability for the self-assembly of metal clusters compared to those surfaces whose reconstructions occur solely to minimise surface energy, which generally consist of changes in bonding configuration or interatomic distances. As the energy saved by these latter reconstruction types is far less than the driving force behind polar surface reconstructions they can be altered due to substrate-adsorbate interactions, which will destroy the actual mechanism of self assembly itself. We note that one would expect the situation to be markedly different for charged species adsorbed onto the surfaces of polar crystals, as this would alter the crystal polarity, and thus result in alterations of the surface reconstruction. The fact that clusters in close proximity do not merge to form larger clusters at room temperature, coupled to the stability of the reconstruction, presents the possibility that this system may be suitable for the formation of dense arrays of nanoclusters, with uniform size and properties.

The system studied here raises numerous points worth further study. It would first be of interest to investigate whether the Au clusters formed on this oxide surface are indeed catalyticaly active. Elevated temperature STM studies would reveal whether this system possesses a high resistance to sintering, as a result of the strong pinning suggested by this study. Other polar surfaces which exhibit reconstructions involving long range vacancy arrays could also be used for self-assembly of metal clusters. Such templates would be highly favourable compared to surfaces which exhibit reconstructions driven only by surface energy concerns.

4 Conclusions

The $Fe_3O_4(001)$ surface terminates at the octahedral plane, exhibiting a $(\sqrt{2}\times\sqrt{2})$R45° reconstruction. Taking into account both the STM images of the surface and the electrostatic model of polar surfaces leads one to support the model of octahedral termination with a $(\sqrt{2}\times\sqrt{2})$R45° array of O^{2-} vacancies. This proposed vacancy array plays a key role in the binding of Au to the surface during the initial stages of adsorption. Au clusters which are 1 ML in height and roughly spherical, with radius ∼9 Å, are formed. The clusters nucleate at the centre of a $(\sqrt{2}\times\sqrt{2})$R45° surface unit cell which has O^{2-} vacancies at each of the four corners of the cell. The identified site may be favourable purely due to a periodic surface stress or because the identified nucleation site is electron rich, compared to the electron poor state of the vacancy site which, coupled to the electronegativity of Au, could also explain the preference for this site. STM shows that Au clusters in nearest neighbour cells still occupy the same site. They do not coalesce and maintain a periodicity inkeeping with the substrate reconstruction. This suggests that it is the periodic potential of the substrate, as opposed to cluster-cluster interactions, which inhibits the coalescence of Au clusters. The stablility of the $(\sqrt{2}\times\sqrt{2})$R45° surface reconstruction, despite the adsorption of Au, is due to the fact that the adsorption of charge neutral species leaves the polarity unchanged, and so the surface reconstruction remains stable. As such, magnetite (001), and other polar crystal surfaces which exhibit long range vacancy arrays, could offer extremely stable templates for the self-assembly of metal clusters.

References

[1] Johannes V. Barth, Giovanni Costantini and Klaus Kern, Nature (London) 437, 671 (2005).

[2] Zhi-Pan Liu, Xue-Qing Gong, Jorge Kohanoff, Cristian Sánchez and P. Hu, Phys. Rev. Lett. 91, 266102 (2004).

[3] Angelo Bongiorno and Uzi Landman, Phys. Rev. Lett. 95, 106102 (2005).

[4] N. Lopez, T. V. W. Janssens, B. S. Clausen, Y. Xu, M. Mavrikakis, T. Bligaard and J. K. Nørskov, J. Catal. 223, 232 (2004).

[5] L. Giordano, J. Goniakowski and G. Pacchioni, Phys. Rev. B 64, 075417 (2001).

[6] Zongxian Yang, Ruqian Wu, Qiming Zhang and D. W. Goodman, Phys. Rev. B 65, 155407 (2002).

[7] José A. Rodriguez, Jan Hrbek, Zhipeng Chang, Joseph Dvorak, Thomas Jirsak and Amitesh Maiti, Phys. Rev. B 65, 235414 (2002).

[8] E. Wahlström, N. Lopez, R. Schaub, P. Thostrup, A. Rønnau, C. Afich, E. Lægsgaard, J. K. Nørskov and F. Besenbacher, Phys. Rev. Lett. 90, 026101 (2003).

[9] L. Giordano, C. Di Valentin, J. Goniakowski and G. Pacchioni, Phys. Rev. Lett. 92, 096105 (2004).

[10] W. T. Wallace, B. K. Min and D. W. Goodman, J. Mol. Catal. A 228, 3 (2005).

[11] Devina Pillay and Gyeong S. Hwang, Phys. Rev. B 72, 205422 (2005).

[12] Y. D. Kim, J. Stultz, T. Wei and D. W. Goodman, J. Phys. Chem. B 106, 6827 (2002).

[13] F. Esch, S. Fabris, L. Zhou, T. Montini, C. Africh, P. Fornasiero, G. Comelli and R. Rosei, Science 309, 752 (2005).

[14] B. Yoon, H. Häkkinen, U. Landman, A. S. Wörz, J-M. Antonietti, S. Abbet, K. Judai and U. Heiz, Science 307, 403 (2005).

[15] H. Brune, M. Giovannini, K. Bromann and K. Kern, Nature (London) 394, 451 (1998).

[16] C. Becker, A. Rosehahn, A. Wiltner, K. von Bergmann, J. Schneider, P. Pervan, M. Milun, M. Kraij and K. Wandelt, New J. Phys. 4, 75.1 (2002).

[17] P.W. Tasker, J. Phys. C 12, 4977 (1979).

[18] P.W. Tasker, Philos. Mag. A 12, 4977 (1979).

[19] B. Stanka, W. Hebenstreit, U. Diebold and S.A. Chambers, Surf. Sci. 448, 49 (2000).

[20] R. Koltun, M. Herrman, G. Güntherodt and V. A. M. Brabers, Appl. Phys. A 73, 49 (2001).

[21] G. Mariotto, S. Murphy and I.V. Shvets, Phys. Rev. B 66, 245426 (2002).

[22] M. Fonin, R. Pentcheva, Yu. S. Dedkov, M. Sperlich, D. V. Vyalikh, M. Scheffler, U. Rüdiger, and G. Güntherodt, Phys. Rev. B 72, 104436 (2005).

[23] C. Cheng, Phys. Rev. B 71, 052401 (2005).

[24] R. Pentcheva, F. Wendler, H. L. Meyerheim, W. Moritz, N. Jedrecy and M. Scheffler, Phys. Rev. Lett. 94, 126101 (2005).

[25] F.C. Voogt, T. Fujii, P.J.M. Smulders, L. Niesen, M.A. James and T. Hibma, Phys. Rev. B 60, 11193 (1999).

[26] I. V. Shvets, G. Mariotto, K. Jordan, N. Berdunov, R. Kantor and S. Murphy, Phys. Rev. B 70, 155406 (2004).

[27] S. F. Ceballos, G. Mariotto, S. Murphy, and I. V. Shvets, Surf. Sci. 131-140, 523 (2003).

[28] K. Jordan, G. Mariotto, S. F. Ceballos, S. Murphy and I.V. Shvets, J. Magn. and Magn. Mater. 290-291, 1029 (2005).

[29] S. F. Alvarado, M. Erbudak and P. Munz, Phys. Rev. B 14, 2740 (1976).

[30] K. Jordan, A. Cazacu, G. Manai, S. F. Ceballos, S. Murphy and I. V. Shvets (in preparation).

[31] B. K. Min, W. T. Wallace and D. W. Goodman, Surf. Sci. L7-L11, 600 (2006).

[32] www.webelements.com

[33] Niklas Nilius, Emile D. L. Rienks, Hans-Peter Rust and Hans-Joachim Freund, Phys. Rev. Lett. 95, 066101 (2005).

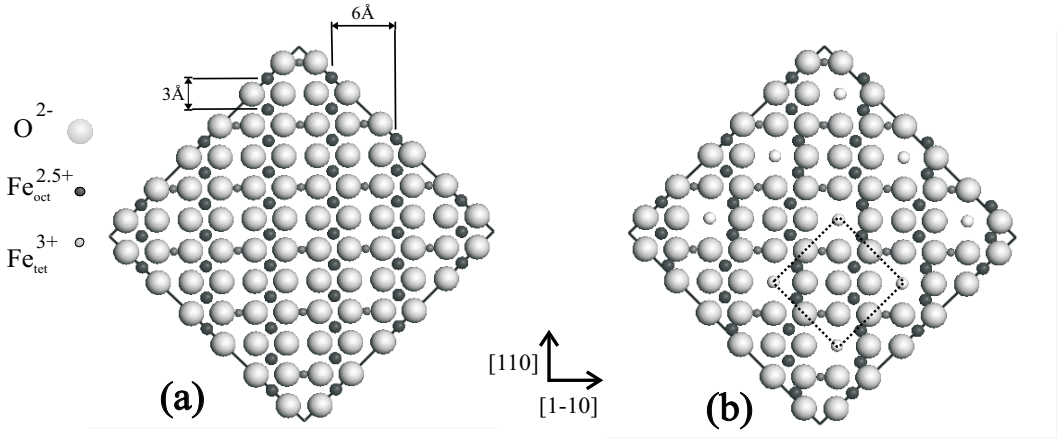

Fig. 1. (a): Schematic of the unreconstructed $Fe_3O_4(001)$ octahedral surface. Fe atoms form straight rows, oriented along the [110] direction. The periodicity along the rows is 3 Å and between them is 6 Å. (b): Oxygen vacancy model proposed first by Voogt [25], and later refined by Stanka [19], to explain first the $(\sqrt{2} \times \sqrt{2})$R45° symmetry and later also the observed wave-like structure of the [110] oriented Fe rows observed in STM. This proposed termination takes into account the polar nature of magnetite (001). The $(\sqrt{2} \times \sqrt{2})$R45° reconstructed unit cell, marked with the black dashed square, is 8.4×8.4 $Å^2$. The four corners of the cell outlined here are centred on oxygen vacancies. The atoms revealed underneath these vacancies are the Fe_{oct} atoms of the underlying octahedral plane.

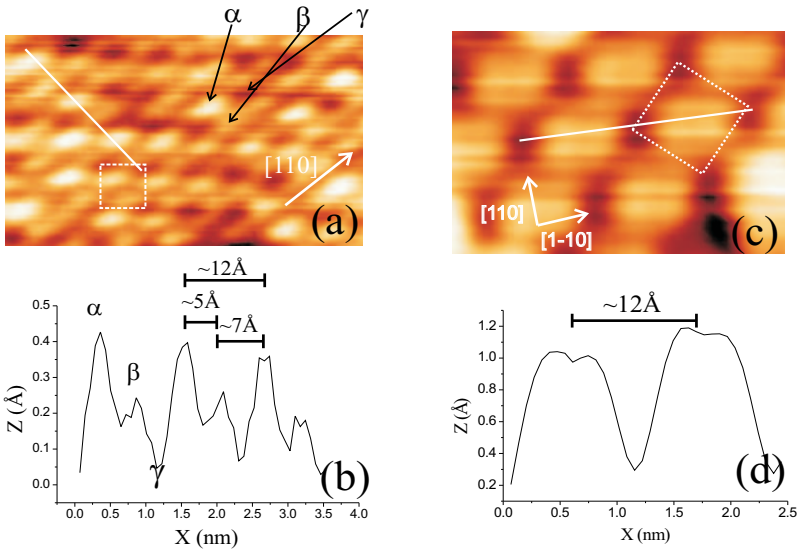

Fig. 2. (a): A 65×45 Å^2 STM image of the surface, obtained with a MnNi STM tip, V_b= +1 V, I_t= 0.1 nA. Spots of two different brightness levels are imaged, labelled α and β. A $(\sqrt{2} \times \sqrt{2})$R45° array of local minima, labelled γ, are also imaged. The unit cell is outlined with the dashed white square. The four corners of the cell are positioned at local minima (γ). (b): Line profile along the white line in (a), illustrating the different intensity of the bright points. The wavelike structure of the Fe rows is also evident, as instead of rows separated by 6Å along the $[1\bar{1}0]$ direction, as one would expect from the bulk structure, the distance between the spots along $[1\bar{1}0]$ alternates between 5Å and 7Å. (c): 35×22 Å^2 STM image, W tip, V_b= -1 V, I_t= 0.1 nA. W tips also image the $(\sqrt{2} \times \sqrt{2})$R45° symmetry. Instead of discreetly resolving the two bright points of different intensity (α and β), only one larger point (which is essentially a combined point instead of two bright points), is resolved. The array of local minima (γ) is resolved as before. The $(\sqrt{2} \times \sqrt{2})$R45° unit cell, again with four local minima at the corners, is outlined with a dashed white square. (d): Due to the fact that individual dimers are not discretely resolved using W tips, the STM images obtained, suggest an apparent 12 Å periodicity, as seen by the line profile taken along the white line in (c). The larger corrugation height for −1V compared to +1V is also evident from this profile.

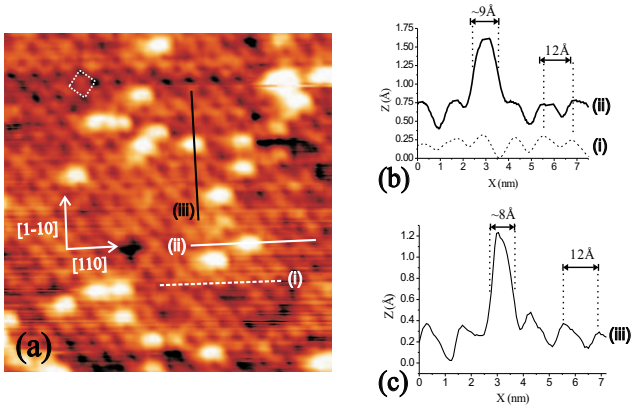

Fig. 3. (a): 150×150 Å^2 STM image, V_b= +1 V, I_t= 0.1 nA, of the $(\sqrt{2} \times \sqrt{2})$R45° reconstructed magnetite surface following deposition of Au onto the surface. The $(\sqrt{2} \times \sqrt{2})$R45° unit cell is denoted by the dashed white square. Uniformly sized Au clusters form on the surface. (b): Dashed white line is a profile along an area without a Au cluster, showing the apparent 12 Å periodicity expected for the clean surface. Whole white line is an equivalent line profile over an area with a Au cluster present. The Au clusters nucleate at points corresponding to a maxima for the clean surface. (c): The same is found for profiles along the perpendicular direction. The maxima where the Au clusters nucleate correspond to the centre of the outlined $(\sqrt{2} \times \sqrt{2})$R45° unit cell. The profiles also show the clusters to have a radius ∼9 Å, however, with some slight elongation evident. The clusters have an apparent height ∼1 Å.

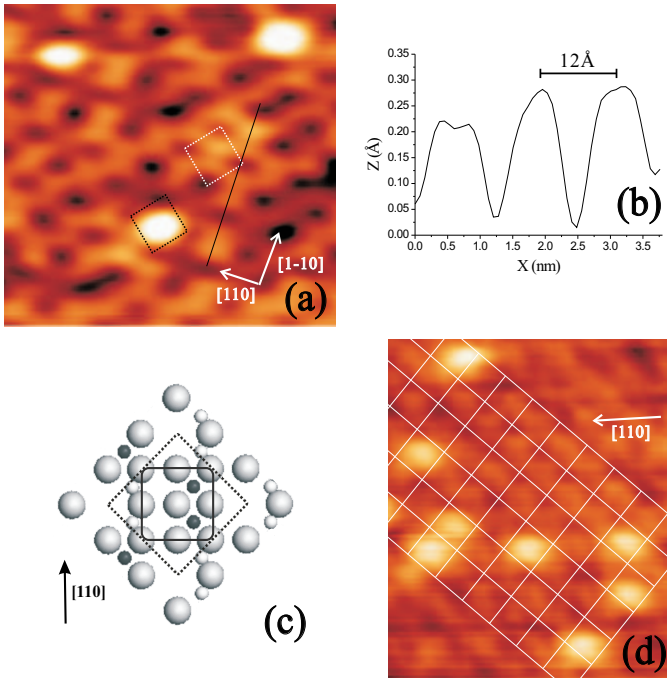

Fig. 4. (a): 70×70 Å^2 STM image, V_b= +1 V, I_t= 0.1 nA, of Au clusters on the $(\sqrt{2} \times \sqrt{2})$R45° reconstructed magnetite (001) surface. The white square outlines a 8.4×8.4 Å^2 surface unit cell. The black square also outlines a unit cell, with a Au cluster nucleated at its centre. (b): Line profile showing the apparent 12 Å periodicity of the magnetite (001) substrate. (c): Model of the cluster nucleation. The cluster (whole grey square) nucleates in the region of the centre of the reconstructed surface unit cell (dashed black square), which has O^{2-} vacancies at the four corners. The charge ordered dimerisation of the Fe_{oct} atoms is incorporated into the schematic. (d): 70×85 Å^2 STM image with a mesh of $(\sqrt{2} \times \sqrt{2})$R45° unit cells superimposed over the image. The Au clusters are always at the centre of the cells.

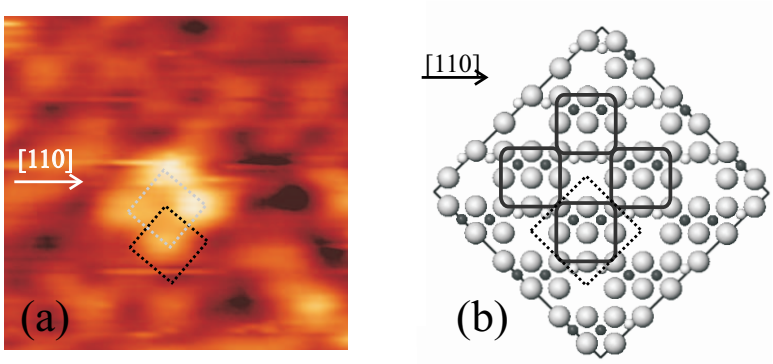

Fig. 5. (a): 65×65 Å^2 image, V_b= +1 V, I_t= 0.1 nA, of four Au clusters occupying neighbouring centre cell sites. The dashed black square is a 8.4×8.4 Å^2 $(\sqrt{2} \times \sqrt{2})$R45° surface unit cell. The clusters are still individually resolved, occupying the previously identified site. (b): Schematic of this structure. Grey squares represent the nucleation area of the Au clusters, and the dashed black square is the same $(\sqrt{2} \times \sqrt{2})$R45° unit cell as represented by the dashed black square in (a).